Engineering Analysis with Boundary Elements 193 (2026) 107064

Contents lists available at ScienceDirect

Engineering Analysis with Boundary Elements

journal homepage: www.elsevier.com/locate/enganabound

Multinode Shepard collocation method for pricing of financial derivatives ☆

Francesco Dell'Accio [a], Filomena Di Tommaso [a,*], Elisa Francomano [b], Clara Lorenzi [a]

[a] Department of Mathematics and Computer Science, University of Calabria, Rende (CS), Italy
[b] Department of Engineering, University of Palermo, Palermo, Italy

ARTICLE INFO

Keywords:
Pricing of financial derivatives
Approximation by rational functions
Multinode Shepard method
Collocation method
Backward differentiation formula

ABSTRACT

This paper explores the use of the multinode Shepard method for the numerical solution of the two-dimensional Black–Scholes equation. The proposed approach combines a spatial approximation based on the multinode Shepard operator with a temporal discretization based on the Backward Differentiation Formula. Numerical experiments assess the accuracy, robustness, and computational properties of the method.

Particular attention is devoted to the behavior of the MS spatial discretization in the presence of the original non-smooth basket payoff and to its sensitivity to the geometry of the node set. The method is compared with both a global RBF collocation approach and a local sparse RBF-FD benchmark. Tests on uniform, Halton, and locally refined node sets show a clear separation between kink-dominated global errors and very high accuracy in smooth regions, together with a marked robustness with respect to changes in node geometry.

1. Introduction

The financial markets are becoming increasingly complex, with not only equities but also numerous types of derivative financial instruments being traded. The market requires up-to-date information on the values of these derivatives every second of every day. This leads to a huge demand for fast and accurate computer simulations [1]. Among the best-known and most widely used models is the Black–Scholes equation, introduced in 1973 by Fischer Black and Myron Scholes, which revolutionized quantitative finance by providing a theoretical framework for option pricing [2]. Although the original formulation of the Black–Scholes equation is one-dimensional, the increasing complexity of financial products has necessitated the development of more advanced models capable of describing multivariate phenomena [3]. One of the most widely used approaches to option pricing is the Finite Difference (FD) method [4]. This method achieves high accuracy and exhibits good convergence properties, although it may involve a significant computational cost, especially in the multi-asset case. Efficient numerical approaches for the PDE formulation include adaptive FD methods [5–7], high-order compact schemes [8,9], Alternating Direction Implicit (ADI) methods [10,11], radial basis function (RBF) approximations [12,13], radial basis function partition of unity (RBF-PU) methods [14–16], and radial basis function generated finite differences (RBF-FD) methods [17,18]. In [19,20], several numerical methods for option pricing are implemented and compared. In [13], it is shown that the RBF method performs competitively with adaptive FD schemes, while in [16] a RBF-PU method is introduced to overcome the main limitation of global RBF approaches, namely the dense and ill-conditioned nature of the collocation matrix. Moreover, the partition of unity framework naturally allows parallel implementation, improving computational efficiency.

Within the meshfree literature for option pricing, it is useful to distinguish the spatial discretization considered here from two RBF-based paradigms that are particularly relevant for comparison. Global RBF collocation represents the numerical solution through globally supported radial kernels; in multidimensional option pricing, adapted node placement can considerably improve the accuracy, but the resulting matrices are dense and the choice of the RBF shape parameter plays a central role in accuracy and conditioning [12,13]. RBF-FD methods follow a different strategy: local RBF-generated differentiation formulas are assembled into sparse differentiation matrices. In particular, the high-order RBF-FD approach in [1] combines polyharmonic splines and polynomials on local stencils. The multinode Shepard (MS) construction investigated in this paper is structurally different from both approaches: it combines local polynomial interpolants defined on unisolvent subsets through rational multinode Shepard weights, leading to a cardinal meshfree collocation framework without constructing either a global RBF expansion or RBF-generated finite-difference stencils.

A significant source of difficulty in option pricing problems is the reduced regularity of the solution induced by the payoff. In particular, for

☆ This article is part of a Special issue entitled: 'Kernel Methods' published in Engineering Analysis with Boundary Elements.

* Corresponding author.
E-mail addresses: francesco.dellaccio@unical.it (F. Dell'Accio), filomena.ditommaso@unical.it (F. Di Tommaso), elisa.francomano@unipa.it (E. Francomano), claralorenzi79@gmail.com (C. Lorenzi).

https://doi.org/10.1016/j.enganabound.2026.107064
Received 30 December 2025; Received in revised form 17 September 2026; Accepted 17 September 2026
0955-7997/© 2026 The Authors. Published by Elsevier Ltd. This is an open access article under the CC BY-NC-ND license (http://creativecommons.org/licenses/by-nc-nd/4.0/).

basket options, the solution typically exhibits a kink along a line in the spatial domain, across which derivatives are discontinuous. This feature can strongly affect the performance of numerical methods and makes such problems a meaningful benchmark for assessing robustness and accuracy. The loss of convergence caused by non-smooth initial data is well known in option pricing. For example, within the high-order RBF-FD framework of [1], a smoothed-payoff variant is considered in order to recover the formal spatial order. In the present study, by contrast, the original non-smooth payoff is deliberately retained. This makes it possible to quantify how the kink affects the MS discretization and to distinguish the kink-dominated global error from the approximation behavior in the smooth part of the computational domain.

The multinode Shepard method - a meshless partition of unity technique based on weighted interpolation [21] - has been previously developed and successfully applied by the authors to elliptic problems and related models [22–25]. The present work extends the MS collocation framework from the previously studied stationary elliptic setting to a time-dependent two-dimensional Black–Scholes problem involving variable coefficients, a mixed second derivative, degeneracy on the coordinate axes, and a non-smooth initial payoff. Neither the Black–Scholes model nor the BDF2 time integrator is claimed as a methodological novelty; the scientific question addressed here is how the MS spatial discretization behaves in this different PDE regime and which numerical features distinguish it from previously studied meshfree approaches. To this end, we combine the multinode Shepard spatial discretization with a standard second-order Backward Differentiation Formula (BDF2) for time integration, which is commonly used in this context due to its stability properties [1,13,26]. This choice allows us to focus on the spatial approximation, which represents the main object of investigation. The contribution of this work lies in the assessment of the multinode Shepard method in a financial context characterized by reduced regularity. In particular, we perform a systematic numerical study of its convergence behavior with respect to spatial refinement, analyze the influence of node distributions, and compare the results with two meshfree benchmarks: a global RBF collocation method [12, 13] and a local sparse RBF-FD-PHS discretization based on Milovanović and von Sydow [1]. For the latter, we use polyharmonic splines r^9, polynomial augmentation of degree $p = 4$, and local stencils of $m = 75$ nodes. To isolate the effect of the spatial discretization, the original non-smooth payoff and the same temporal discretization employed in the MS experiments are retained for the RBF-FD benchmark. The shape parameter of the global RBF method is determined through Leave-One-Out Cross-Validation (LOOCV). The sensitivity to node geometry is examined on uniform layouts, scattered Halton sets, and strongly locally refined configurations. The purpose of this comparison is therefore not merely to show the benefit of a particular adapted distribution, but to assess whether the MS discretization remains reliable under substantial changes in the geometry of the node set. The numerical results show that the global error is strongly influenced by the region near the payoff kink, which limits the observation of classical convergence rates. However, when the error is evaluated away from the kink, the multinode Shepard method achieves a significant improvement in accuracy. Moreover, the method exhibits a high robustness with respect to irregular and locally refined node distributions. The comparison with RBF-FD provides an additional local sparse benchmark, allowing the effects of locality and sparsity to be distinguished from those specific to the MS approximation. Accordingly, the main numerical insight is not a claim of universal superiority over existing option-pricing schemes, but the identification of a characteristic combination of very high accuracy in smooth regions and robustness with respect to node geometry, while the unsmoothed payoff remains the dominant source of the global error.

The paper is organized as follows. Section 2 recalls the multinode Shepard method, focusing on its main definitions and properties. Section 3 introduces the two-dimensional Black–Scholes model. Section 4 is devoted to the spatial discretization, while Section 5 presents the temporal discretization based on BDF2 schemes. Section 6 reports the numerical experiments and compares different node distributions. The convergence analysis is discussed in Section 6.3. Finally, conclusions are drawn in Section 7

2. The multinode Shepard method

Let $X = \{\mathbf{x}_1, \dots, \mathbf{x}_n\}$ be a set of n pairwise distinct points in a domain $\Omega \subset \mathbb{R}^s$ with associated data f_i sampled from an unknown function $f : \Omega \to \mathbb{R}$, that is $f_i = f(\mathbf{x}_i)$, $i = 1, \dots n$. Let $p \in \mathbb{N}$ and let us denote by $\mathbb{P}_p(\mathbb{R}^s)$ the space of polynomials in s variables of total degree p, of dimension $\tau = \binom{s+p}{s}$.

Let us assume that a covering $\mathcal{T} = \{t_1, \dots, t_m\}$ of the set X is given, where each subset t_j has cardinality τ and is unisolvent for interpolation by polynomials in $\mathbb{P}_p(\mathbb{R}^s)$. We set $t_j = \{\mathbf{x}_{j_k} \mid k = 1, \dots, \tau\}$ and denote by $p_j[f] \in \mathbb{P}_p(\mathbb{R}^s)$ the unique polynomial such that $p_j[f](\mathbf{x}_{j_k}) = f(\mathbf{x}_{j_k})$.

The multinode Shepard operator, associated to the covering $\mathcal{T}$, is then defined by

$$\mathcal{M}_\mu[f](\mathbf{x}) = \sum_{j=1}^{m} B_{\mu,j}(\mathbf{x})\, p_j[f](\mathbf{x}), \quad \mu > 0, \quad \mathbf{x} \in \mathbb{R}^s, \tag{1}$$

where

$$B_{\mu,j}(\mathbf{x}) = \frac{\prod_{\ell=1}^{\tau} \left\|\mathbf{x} - \mathbf{x}_{j_\ell}\right\|^{-\mu}}{\sum_{k=1}^{m} \prod_{\ell=1}^{\tau} \left\|\mathbf{x} - \mathbf{x}_{k_\ell}\right\|^{-\mu}}, \quad j = 1, \dots, m, \tag{2}$$

are the multinode Shepard functions, generalizing the Little triangular Shepard functions [27]. These functions satisfy the following properties:

1. $\sum_{j=1}^{m} B_{\mu,j}(\mathbf{x}) = 1$,
2. $B_{\mu,j}(\mathbf{x}_i) = 0$ for all $\mathbf{x}_i \notin t_j$,
3. $\nabla B_{\mu,j}(\mathbf{x}_i) = \mathbf{0}$, $\mu > 1$,
4. $\mathrm{H}\, B_{\mu,j}(\mathbf{x}_i) = \mathbf{0}$, $\mu > 2$,
5. $\sum_{j \in \mathcal{J}_i} B_{\mu,j}(\mathbf{x}_i) = 1$,
6. $\sum_{j \in \mathcal{J}_i} \nabla B_{\mu,j}(\mathbf{x}_i) = \mathbf{0}$, $\mu > 1$,
7. $\sum_{j \in \mathcal{J}_i} \mathrm{H}\, B_{\mu,j}(\mathbf{x}_i) = \mathbf{0}$, $\mu > 2$,

where $\nabla B_{\mu,j}(\mathbf{x})$ and $\mathrm{H}\, B_{\mu,j}(\mathbf{x})$ are the gradient and the Hessian matrix of $B_{\mu,j}(\mathbf{x})$ and $\mathcal{J}_i = \{j \in \{1, \dots, m\} : i \in \{j_1, \dots, j_\tau\}\}$ is the set of indices of the τ-tuples t_j which contain the point $\mathbf{x}_i$.

In applying the multinode Shepard operator, it is convenient to express the local polynomial interpolants in (1) in barycentric form

$$p_j[f](\mathbf{x}) = \sum_{i=1}^{\tau} \lambda_{j,i}(\mathbf{x})\, f_{j_i}, \tag{3}$$

where $\lambda_{j,i}(\mathbf{x})$ are the fundamental Lagrange polynomials related to the subsets t_j, satisfying the condition

$$\lambda_{j,i}\left(\mathbf{x}_{j_k}\right) = \begin{cases} 1, & i = k, \\ 0, & \text{otherwise.} \end{cases} \tag{4}$$

After a rearrangement, it is possible to rewrite the operator $\mathcal{M}_\mu[f]$ in terms of the function values

$$\mathcal{M}_\mu[f](\mathbf{x}) = \sum_{i=1}^{n} \sum_{j \in \mathcal{J}_i} B_{\mu,j}(\mathbf{x})\, \lambda_{j,i}(\mathbf{x})\, f_i = \sum_{i=1}^{n} W_{\mu,i}(\mathbf{x})\, f_i.$$

We notice that the functions

$$W_{\mu,i}(\mathbf{x}) = \sum_{j \in \mathcal{J}_i} B_{\mu,j}(\mathbf{x})\, \lambda_{j,i}(\mathbf{x}) \tag{5}$$

constitute a cardinal basis and we refer to it as the multinode cardinal Shepard basis (for more details see [22–25]).

3. The Black–Scholes problem

From the mathematical point of view, the multi-dimensional Black–Scholes equation takes the form [1]

$$\begin{cases} \dfrac{\partial}{\partial \hat{t}} P(\hat{t}, \mathbf{x}) = \mathcal{L} P(\hat{t}, \mathbf{x}), \quad \hat{t} \in \mathbb{R}_+, \ \mathbf{x} \in \mathbb{R}^s_+, \\ P(0, \mathbf{x}) = \Phi(\mathbf{x}), \quad \mathbf{x} \in \mathbb{R}^s_+, \end{cases} \tag{6}$$

where

$$\mathcal{L}P = r\sum_{i=1}^{s} x_i \frac{\partial P}{\partial x_i} + \frac{1}{2}\sum_{i,j=1}^{s} \sigma_i\sigma_j\rho_{ij}x_i x_j \frac{\partial^2 P}{\partial x_i \partial x_j} - rP, \tag{7}$$

with $P\left(\hat{t},\mathbf{x}\right)$ being the value of the option at time $\hat{t}$ when the underlying assets have the values specified by $\mathbf{x} = (x_1,\dots,x_s)$. The coefficient r in Eq. (7) denotes the scaled short interest rate, σ_i is the volatility of the asset i, ρ_{ij} is the correlation between assets i and j, and the upper limit s of the sums indicates the number of underlying assets, which corresponds to the number of spatial dimensions in the problem. A common example of a contract function for a European basket call option is the average option, mathematically expressed as

$$\Phi(\mathbf{x}) = \max\left(\frac{1}{s}\sum_{i=1}^{s} x_i - K, 0\right),$$

where $K \in \mathbb{R}$ is the strike price. The special case of the two-dimensional Black–Scholes equation, which is the objective of investigation of the present paper, is useful in pricing options that depend on two underlying assets or in scenarios where there is greater interaction between variables [28]. For simplicity, we set $(x_1, x_2) = (x, y)$ and Eq. (7) becomes

$$\begin{aligned}\mathcal{L}P = {} & r\left(x\frac{\partial P}{\partial x} + y\frac{\partial P}{\partial y}\right) + \frac{1}{2}\left(\sigma_1^2x^2\frac{\partial^2 P}{\partial x^2} + \sigma_2^2y^2\frac{\partial^2 P}{\partial y^2}\right)\\ & + \rho\sigma_1\sigma_2 xy\frac{\partial^2 P}{\partial x\partial y} - rP,\end{aligned} \tag{8}$$

where we assume $\rho_{11} = \rho_{22} = 1$ and $\rho_{12} = \rho_{21} = \rho$ [1].

3.1. Boundary conditions

Janson and Tysk in [29] demonstrate that the problem under consideration is well-posed even without explicit boundary conditions, both in space and time, provided that the growth at infinity is suitably restricted. Consequently, we need to restrict the problem to a finite domain and impose only near-field and far-field boundary conditions [1, 13]. The near-field boundary is fixed at the point $x = y = 0$, where the following condition is applied

$$P(0,0,t) = 0, \quad 0 \le t \le T. \tag{9}$$

At the artificial far-field boundary $x + y = 8$, we impose the standard asymptotic basket-call condition

$$P(x,y,t) = \frac{x+y}{2} - Ke^{-rt}, \qquad 0 \le t \le T, \qquad x + y = 8. \tag{10}$$

No additional Dirichlet data are prescribed on the coordinate axes (apart from the origin); axis nodes are treated as PDE collocation nodes, consistently with the degeneracy of the Black–Scholes operator.

4. Spatial approximation

Under the above assumptions, let $\Omega \subset \mathbb{R}^2$ be the triangle of vertices $(0,0)$, $(8,0)$ and $(0,8)$. We assume that a node set $X = \{\mathbf{x}_1,\dots,\mathbf{x}_n\}$ is given together with a covering $\mathcal{T}$ and that the points in X are organized such that $\mathbf{x}_1,\dots,\mathbf{x}_{n_I}$ are collocation points of Ω, $\mathbf{x}_{n_I+1}$ is the origin and $\mathbf{x}_{n_I+2},\dots,\mathbf{x}_n$ are points on the boundary line $x + y = 8$.

We assume that the solution of the problem (6) subject to the boundary conditions (9) and (10) is approximated, at a fixed time step t, by a multinode Shepard operator $\mathcal{M}_\mu[P;t](\mathbf{x})$. Consequently, by imposing the differential conditions (8), we have

$$\begin{aligned}\mathcal{L}P \approx {} & \mathcal{L}\mathcal{M}_\mu[P;t](\mathbf{x})\\ = {} & r\left(x\frac{\partial \mathcal{M}_\mu}{\partial x}(\mathbf{x}) + y\frac{\partial \mathcal{M}_\mu}{\partial y}(\mathbf{x})\right)\\ & + \frac{1}{2}\left(\sigma_1^2x^2\frac{\partial^2 \mathcal{M}_\mu}{\partial x^2}(\mathbf{x}) + \sigma_2^2y^2\frac{\partial^2 \mathcal{M}_\mu}{\partial y^2}(\mathbf{x})\right)\\ & + \rho\sigma_1\sigma_2 xy\frac{\partial^2 \mathcal{M}_\mu}{\partial x\partial y}(\mathbf{x}) - r\mathcal{M}_\mu(\mathbf{x}),\end{aligned} \tag{11}$$

where, in order to simplify notation, we use $\mathcal{M}_\mu$ instead of $\mathcal{M}_\mu[P;t](x,y)$. By computing the first and second order derivatives of the multinode cardinal basis functions (5), it follows that

$$\begin{aligned}\mathcal{L}\mathcal{M}_\mu(\mathbf{x}) = \sum_{i=1}^{n} \Bigg(& r\left(x\frac{\partial W_{\mu,i}}{\partial x}(\mathbf{x}) + y\frac{\partial W_{\mu,i}}{\partial y}(\mathbf{x})\right)\\ & + \frac{1}{2}\left(\sigma_1^2x^2\frac{\partial^2 W_{\mu,i}}{\partial x^2}(\mathbf{x}) + \sigma_2^2y^2\frac{\partial^2 W_{\mu,i}}{\partial y^2}(\mathbf{x})\right)\\ & + \rho\sigma_1\sigma_2 xy\frac{\partial^2 W_{\mu,i}}{\partial x\partial y}(\mathbf{x}) - rW_{\mu,i}(\mathbf{x})\Bigg)P_i(t),\end{aligned} \tag{12}$$

where $P_i(t) = \mathcal{M}_\mu[P;t](\mathbf{x}_i)$ is the approximation of the solution $P(t,\mathbf{x})$ of the problem (6) at the point $\mathbf{x}_i$.

By evaluating (12) at the collocation points $\mathbf{x}_k = (x_k, y_k)$ and by separating the terms related to the internal points from the ones related to the boundary points, we get the spatial matrices

$$\mathcal{A} = \begin{bmatrix} \mathcal{A}_{1,1} & \dots & \mathcal{A}_{1,n_I} \\ \mathcal{A}_{2,1} & \dots & \mathcal{A}_{2,n_I} \\ \vdots & & \vdots \\ \mathcal{A}_{n_I,1} & \dots & \mathcal{A}_{n_I,n_I} \end{bmatrix}, \qquad \mathcal{B} = \begin{bmatrix} \mathcal{B}_{1,n_I+1} & \dots & \mathcal{B}_{1,n} \\ \mathcal{B}_{2,n_I+1} & \dots & \mathcal{B}_{2,n} \\ \vdots & & \vdots \\ \mathcal{B}_{n_I,n_I+1} & \dots & \mathcal{B}_{n_I,n} \end{bmatrix}$$

with

$$\begin{aligned}\mathcal{A}_{ki} = {} & r\left(x_k\frac{\partial W_{\mu,i}}{\partial x}(\mathbf{x}_k) + y_k\frac{\partial W_{\mu,i}}{\partial y}(\mathbf{x}_k)\right)\\ & + \frac{1}{2}\left(\sigma_1^2x_k^2\frac{\partial^2 W_{\mu,i}}{\partial x^2}(\mathbf{x}_k) + \sigma_2^2y_k^2\frac{\partial^2 W_{\mu,i}}{\partial y^2}(\mathbf{x}_k)\right)\\ & + \rho\sigma_1\sigma_2x_ky_k\frac{\partial^2 W_{\mu,i}}{\partial x\partial y}(\mathbf{x}_k) - rW_{\mu,i}(\mathbf{x}_k),\\ & k = 1,\dots,n_I,\ i = 1,\dots,n_I,\end{aligned} \tag{13}$$

$$\begin{aligned}\mathcal{B}_{ki} = {} & r\left(x_k\frac{\partial W_{\mu,i}}{\partial x}(\mathbf{x}_k) + y_k\frac{\partial W_{\mu,i}}{\partial y}(\mathbf{x}_k)\right)\\ & + \frac{1}{2}\left(\sigma_1^2x_k^2\frac{\partial^2 W_{\mu,i}}{\partial x^2}(\mathbf{x}_k) + \sigma_2^2y_k^2\frac{\partial^2 W_{\mu,i}}{\partial y^2}(\mathbf{x}_k)\right)\\ & + \rho\sigma_1\sigma_2x_ky_k\frac{\partial^2 W_{\mu,i}}{\partial x\partial y}(\mathbf{x}_k) - rW_{\mu,i}(\mathbf{x}_k),\\ & k = 1,\dots,n_I,\ i = n_I+1,\dots,n.\end{aligned} \tag{14}$$

5. Temporal discretization

The temporal discretization is performed by means of a second-order Backward Differentiation Formula (BDF2), which provides a stable and accurate approximation of the time derivative [1]. Since BDF2 is a multistep method, a first-order scheme is used to compute the first time step. This initialization does not affect the overall second-order accuracy of the method. In the MATLAB implementation and in all numerical experiments, the time grid is uniform:

$$t^n = n\Delta t, \qquad \Delta t = \frac{T}{M}, \qquad n = 0,\dots,M.$$

We denote by

$$\mathbf{P}_I^n = [P_1^n,\dots,P_{n_I}^n]^T$$

the vector of unknown nodal values at the n_I PDE-collocation nodes. The boundary vector at time t^n is

$$\mathbf{b}^n = [b_{n_I+1}^n,\dots,b_n^n]^T,\ b_{n_I+1}^n = 0,\ b_i^n = \frac{x_i+y_i}{2} - Ke^{-rt^n}, \quad i = n_I+2,\dots,n. \tag{15}$$

The initial condition is sampled at the collocation nodes,

$$\mathbf{P}_I^0 = [\Phi(\mathbf{x}_1),\dots,\Phi(\mathbf{x}_{n_I})]^T. \tag{16}$$

A Backward Euler step is used for initialization. With the spatial matrices (13)–(14), it reads

$$(\mathbf{I} - \Delta t\,\mathcal{A})\,\mathbf{P}_I^1 = \mathbf{P}_I^0 + \Delta t\,\mathcal{B}\mathbf{b}^1. \tag{17}$$

For $n = 2, \dots, M$, the constant-step BDF2 formula gives

$$\left(\mathbf{I} - \frac{2}{3}\Delta t\,\mathcal{A}\right)\mathbf{P}_I^n = \frac{4}{3}\mathbf{P}_I^{n-1} - \frac{1}{3}\mathbf{P}_I^{n-2} + \frac{2}{3}\Delta t\,\mathcal{B}\mathbf{b}^n. \tag{18}$$

Here $\mathbf{I}$ is the $n_I \times n_I$ identity matrix. Since both $\mathcal{A}$ and Δt are time independent, the coefficient matrix in (18) is the same at every BDF2 step and can be factorized once and reused throughout the time integration. Notice in particular that the boundary vector is time dependent, $\mathbf{b}^n$, through the discounted strike term Ke^{-rt^n}.

6. Numerical results

6.1. Comparison of node distributions

All numerical tests in this section use the original, unsmoothed basket payoff. This choice is deliberate: the aim is to assess separately the behavior of the spatial discretizations in the low-regularity region and in the smooth part of the domain, rather than to recover a formal high-order rate by regularizing the initial data.

In this section, we investigate the performance of different node distributions in order to assess the accuracy, stability, and sensitivity of the considered meshfree discretizations with respect to the node geometry. The parameters of the Black–Scholes model are fixed as follows: $\sigma_1 = \sigma_2 = 0.15$, $r = 0.03$, $\rho = 0.5$, $K = 1$, and $T = 0.045$. The time interval $[0, T]$ is discretized using $M = 20$ uniform time steps, with $\Delta t = T/M$.

For each time step t^ℓ, $\ell = 1, \dots, M$, we evaluate the mean absolute error

$$E_{\text{mean}}(t^\ell) = \frac{1}{n_{\text{eval}}} \sum_{i=1}^{n_{\text{eval}}} \left|\tilde{u}(\boldsymbol{\xi}_i, t^\ell) - u^*(\boldsymbol{\xi}_i, t^\ell)\right|,$$

and the maximum absolute error

$$E_{\max}(t^\ell) = \max_{1 \le i \le n_{\text{eval}}} \left|\tilde{u}(\boldsymbol{\xi}_i, t^\ell) - u^*(\boldsymbol{\xi}_i, t^\ell)\right|.$$

Here, u^* denotes a reference solution computed by means of a second-order finite difference scheme. Specifically, the reference computation uses 200 grid points in each spatial direction on the Cartesian square $[0, 8]^2$ and a temporal refinement of $N_t = 20M$ time steps (thus $N_t = 400$ for the standard choice $M = 20$); the error is then evaluated at the points belonging to the triangular computational domain. The quantity $\tilde{u}(\boldsymbol{\xi}_i, t^\ell)$ denotes the numerical approximation provided by MS, global RBF collocation, or RBF-FD, and $\{\boldsymbol{\xi}_i\}_{i=1}^{n_{\text{eval}}}$ is the set of evaluation points uniformly distributed over the triangular domain. In addition to accuracy, we monitor the conditioning of the matrices arising from the time-discrete problems.

The approximations are computed using representative node distributions. In particular, we consider uniform and Halton node sets as baseline configurations, and a problem-adapted distribution obtained by locally refining the nodes in a neighborhood of the payoff kink line $x + y = 2K$. For MS, the degree of the local polynomial interpolant is fixed to $p = 2$ and the exponent is set to $\mu = 4$. Preliminary tests with finer temporal discretizations showed that, for the considered time horizon, the overall error is mainly governed by the spatial approximation.

The covering $\mathcal{T}$ used by MS is constructed by means of the adaptive procedure in [30, Algorithm 2]. The node set is first partitioned according to the line $x + y = 2K$. For each subset, local neighborhoods are defined through square regions of increasing size, ensuring the inclusion of a sufficient number of nodes. The points are then ordered by distance from the center and a subset of six nodes is selected via a Leja-type strategy based on a pivoted LU factorization of the local Vandermonde matrix [31]. This guarantees unisolvence and improves the stability of the local polynomial approximation.

Two RBF-based benchmarks are considered. The first is a global multiquadric RBF collocation method of Kansa type, coupled with the same BDF2 time discretization [12,13]. Its shape parameter ϵ is selected by minimizing a Leave-One-Out Cross-Validation (LOOCV) criterion through the cost-effective Rippa procedure, in order to avoid an arbitrary or manually tuned parameter choice.

The second benchmark is the local sparse RBF-FD discretization proposed for option pricing in [1]. Following that construction, we use polyharmonic splines $\phi(r) = r^9$ augmented with polynomials of degree $p = 4$, and a stencil of $m = 75$ nearest nodes. Unlike the global multiquadric RBF method, this PHS-based RBF-FD formulation does not require the selection of an RBF shape parameter. In the present experiments, only the spatial discretization is taken from the RBF-FD formulation, while the same uniform BDF2 time discretization adopted for MS and global RBF is used. Moreover, the original unsmoothed payoff is retained for all three methods.

In all comparisons, MS, global RBF, and RBF-FD are therefore tested on the same node sets, with the same Black–Scholes parameters, temporal discretization, reference solution, and evaluation points. This setup is intended to isolate, as far as possible, the effect of the spatial approximation from that of the node distribution and the time integrator.

6.1.1. Halton vs. uniform node distributions

We first compare the three spatial discretizations on uniform and Halton node sets of comparable size, in order to assess the influence of the node geometry on accuracy and numerical stability. Figs. 1 and 2 show the two node configurations together with the absolute error surfaces at the last time step for global RBF, RBF-FD, and MS.

Tables 1 and 2 report the time evolution of the mean and maximum errors and the corresponding condition numbers. The corresponding condition numbers are denoted by κ_{RBF}, $\kappa_{\text{RBF-FD}}$, and κ_{MS}, respectively. All three methods exhibit stable error profiles over the considered time interval, with no evidence of temporal instability. However, the sensitivity to the node distribution is markedly different.

On the uniform node set, RBF-FD provides the smallest mean error among the three methods throughout the time integration. At the final time, $E_{\text{mean}} = 9.83 \times 10^{-5}$ for RBF-FD, compared with 1.66×10^{-4} for global RBF and 1.85×10^{-4} for MS. The maximum errors of RBF-FD and global RBF are also of comparable magnitude, approximately 1.6×10^{-2}, whereas MS exhibits a larger localized maximum error of approximately 9.0×10^{-2}.

The behavior changes when the structured node set is replaced by the scattered Halton distribution. The final mean error of RBF-FD increases from 9.83×10^{-5} to 2.76×10^{-4}, while its maximum error increases from 1.57×10^{-2} to 5.36×10^{-2}. Global RBF also exhibits a deterioration, with the final mean error increasing from 1.66×10^{-4} to 2.73×10^{-4}. In contrast, the MS errors remain of comparable magnitude under the change of node geometry: its final mean error changes from 1.85×10^{-4} on uniform nodes to 1.49×10^{-4} on Halton nodes.

A similar trend is visible in the conditioning of the discrete systems. For the BDF2 steps, the condition number associated with RBF-FD increases from about 1.11 on the uniform distribution to about 3.50 on the Halton distribution. The corresponding changes are more moderate for global RBF and MS. Although all the reported values remain numerically manageable, the comparison indicates a greater sensitivity of the RBF-FD discretization to the scattered geometry in the present experiment.

These results also clarify the interpretation of the robustness previously observed for MS. The reduced sensitivity of MS to the node distribution is not only observed relative to the global RBF benchmark, for which local-versus-global support already introduces an important structural difference, but also relative to the local sparse RBF-FD discretization considered here. At the same time, the results do not indicate a uniform accuracy advantage of MS: on the structured uniform set, RBF-FD achieves a smaller global mean error and a substantially smaller global maximum error. The distinguishing feature of MS in this experiment is therefore its limited sensitivity to the change in node geometry, rather than uniform superiority in accuracy.

Table 1
Time evolution of mean and maximum errors for global RBF, RBF-FD, and MS on a set of $n_I = 559$ Halton points.

ℓ	$E^{\mathrm{RBF}}_{\mathrm{mean}}$	$E^{\mathrm{RBF}}_{\max}$	κ^{RBF}	$E^{\mathrm{RBF-FD}}_{\mathrm{mean}}$	$E^{\mathrm{RBF-FD}}_{\max}$	$\kappa^{\mathrm{RBF-FD}}$	$E^{\mathrm{MS}}_{\mathrm{mean}}$	$E^{\mathrm{MS}}_{\max}$	κ^{MS}
1	2.87e−4	2.87e−2	1.89	3.03e−4	5.85e−2	5.20	1.26e−4	7.96e−2	1.00
2	2.86e−4	2.86e−2	1.89	3.01e−4	5.82e−2	3.50	1.27e−4	7.97e−2	1.42
3	2.84e−4	2.84e−2	1.89	2.99e−4	5.79e−2	3.50	1.28e−4	7.97e−2	1.42
4	2.83e−4	2.83e−2	1.89	2.97e−4	5.77e−2	3.50	1.29e−4	7.98e−2	1.42
5	2.82e−4	2.82e−2	1.89	2.95e−4	5.74e−2	3.50	1.30e−4	7.99e−2	1.42
6	2.81e−4	2.80e−2	1.89	2.94e−4	5.71e−2	3.50	1.32e−4	7.99e−2	1.42
7	2.80e−4	2.79e−2	1.89	2.92e−4	5.69e−2	3.50	1.33e−4	8.00e−2	1.42
8	2.80e−4	2.78e−2	1.89	2.91e−4	5.66e−2	3.50	1.34e−4	8.00e−2	1.42
9	2.79e−4	2.77e−2	1.89	2.89e−4	5.63e−2	3.50	1.35e−4	8.01e−2	1.42
10	2.78e−4	2.75e−2	1.89	2.88e−4	5.61e−2	3.50	1.37e−4	8.02e−2	1.42
11	2.77e−4	2.74e−2	1.89	2.86e−4	5.58e−2	3.50	1.38e−4	8.02e−2	1.42
12	2.77e−4	2.73e−2	1.89	2.85e−4	5.56e−2	3.50	1.39e−4	8.03e−2	1.42
13	2.76e−4	2.72e−2	1.89	2.84e−4	5.53e−2	3.50	1.40e−4	8.04e−2	1.42
14	2.76e−4	2.71e−2	1.89	2.83e−4	5.51e−2	3.50	1.41e−4	8.04e−2	1.42
15	2.75e−4	2.69e−2	1.89	2.81e−4	5.48e−2	3.50	1.43e−4	8.05e−2	1.42
16	2.75e−4	2.68e−2	1.89	2.80e−4	5.46e−2	3.50	1.44e−4	8.06e−2	1.42
17	2.74e−4	2.67e−2	1.89	2.79e−4	5.43e−2	3.50	1.45e−4	8.06e−2	1.42
18	2.74e−4	2.66e−2	1.89	2.78e−4	5.41e−2	3.50	1.46e−4	8.07e−2	1.42
19	2.73e−4	2.65e−2	1.89	2.77e−4	5.38e−2	3.50	1.47e−4	8.08e−2	1.42
20	2.73e−4	2.63e−2	1.89	2.76e−4	5.36e−2	3.50	1.49e−4	8.09e−2	1.42

In order to examine separately the behavior of the discretizations in the smooth part of the solution, we also evaluate the error away from the payoff kink. We exclude a band of width $\delta = 0.3$ around the line $x + y = 2K$ and compute the errors only at evaluation points satisfying

$$|x + y - 2K| > \delta.$$

The results at the last time step are reported in Table 3.

For the uniform configuration, the away-from-the-kink mean error is 2.18×10^{-4} for global RBF, 6.97×10^{-5} for RBF-FD, and 9.57×10^{-7} for MS. On Halton nodes, the corresponding errors are 3.35×10^{-4}, 2.50×10^{-4}, and 5.80×10^{-7}, respectively. Thus, the MS approximation remains extremely accurate in the smooth region for both node distributions, whereas RBF-FD exhibits a more pronounced sensitivity to the transition from uniform to scattered nodes.

The away-from-the-kink results should, however, be interpreted as a diagnostic of the approximation behavior in smooth regions rather than as evidence of uniformly high accuracy for the option-pricing problem. The largest MS errors remain concentrated in the neighborhood of the payoff kink, corresponding to the at-the-money region, where the reduced regularity is both numerically challenging and financially relevant. The very small errors observed away from this region are consistent with the local polynomial character of the MS construction and its exact reproduction of polynomials up to the degree used in the local approximation. This favorable smooth-region behavior does not remove the deterioration associated with the nonsmooth payoff near the kink.

6.1.2. Effect of local refinement near the kink

We investigate the effect of a locally refined node distribution obtained by increasing the resolution in a neighborhood of the payoff kink $x + y = 2K$. The node set is constructed by combining a coarse background grid with a finer band around the kink, together with additional points located directly on the kink and near the origin. Boundary nodes are included along the line $x + y = 8$. The resulting configuration consists of approximately $n_I = 906$ collocation nodes (see Fig. 3(a)).

To provide a fair comparison, we also consider a uniform node distribution with a similar number of collocation nodes ($n_I = 902$). The results at the final time are reported in Table 4, where both global and away-from-the-kink errors are shown.

The three methods exhibit markedly different sensitivities to local refinement. The global RBF method undergoes a severe deterioration in accuracy, with large errors both globally and away from the kink. In contrast, the local RBF-FD discretization remains stable on the refined node set and achieves errors of the same order as MS in terms of global mean error. Moreover, RBF-FD provides a smaller global maximum error than MS in this configuration.

A different behavior is observed away from the kink. In the smooth region, MS attains significantly smaller mean and maximum errors than both RBF-FD and global RBF. This confirms that the very small MS errors observed away from the kink are not merely a consequence of comparing a local method with a global RBF discretization.

Overall, the results indicate that local refinement does not lead to a uniform improvement for all methods. RBF-FD is considerably more robust to clustering than global RBF, while MS combines a comparable global mean error with a much higher accuracy in the smooth part of the domain. At the same time, the larger global MS error near the payoff kink shows that no uniform accuracy advantage can be claimed.

6.2. Robustness with respect to node distribution and resolution

To assess the robustness with respect to spatial resolution, we consider a sequence of Halton node distributions with an increasing number of interior nodes. The time evolution of the mean error is shown in Fig. 4 for global RBF, RBF-FD, and MS. For all considered node sets, the global RBF and RBF-FD methods exhibit stable error profiles, with a slight decrease over time and a regular improvement as the spatial resolution increases. The MS method also remains stable, although its mean error shows a mild increase during the time integration. Overall, its accuracy improves with increasing node resolution, with the reduction becoming less pronounced for the finer discretizations.

A distinction among the methods emerges when the error is evaluated away from the payoff kink. As shown in Fig. 5, both global RBF and RBF-FD improve under spatial refinement, with RBF-FD giving the smaller error for the finest node sets. The MS method exhibits a much stronger reduction, reaching mean errors of the order of 10^{-9}. These very small values characterize the approximation behavior in the smooth part of the domain and are consistent with the local polynomial reproduction properties of the MS approximation.

6.3. Convergence analysis

In this section, we separately investigate the influence of the temporal and spatial discretizations. The temporal experiment below is intended as a sensitivity check: because the measured errors are already dominated by the spatial discretization, it is not used to estimate the formal BDF2 convergence order.

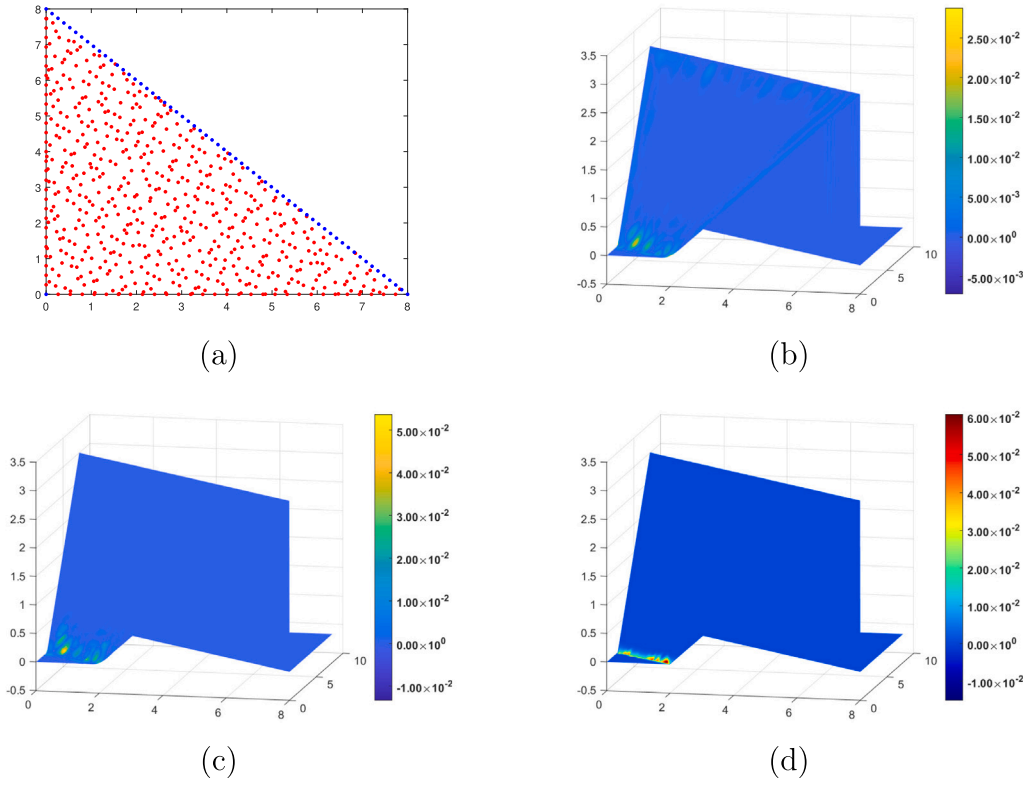

Fig. 1. (a) Set of 559 collocation Halton points coupled with 63 boundary points. Absolute error surface at the last time step for (b) the global RBF method, (c) the RBF-FD method, and (d) the MS method.

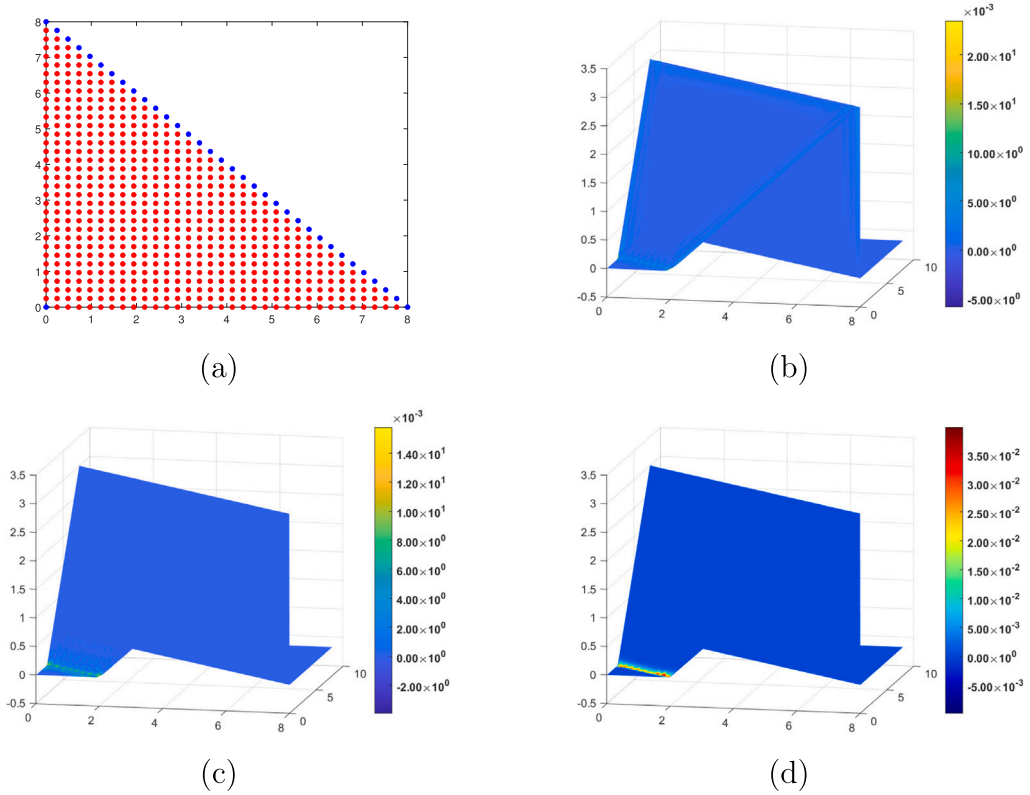

Fig. 2. (a) Set of 560 collocation uniformly distributed nodes coupled with 35 boundary points. Absolute error surface at the last time step for (b) the global RBF method, (c) the RBF-FD method, and (d) the MS method.

Table 2
Time evolution of mean and maximum errors for global RBF, RBF-FD, and MS on a set of $n_I = 560$ uniform points.

ℓ	$E_{\text{mean}}^{\text{RBF}}$	$E_{\text{max}}^{\text{RBF}}$	κ^{RBF}	$E_{\text{mean}}^{\text{RBF-FD}}$	$E_{\text{max}}^{\text{RBF-FD}}$	$\kappa^{\text{RBF-FD}}$	$E_{\text{mean}}^{\text{MS}}$	$E_{\text{max}}^{\text{MS}}$	κ^{MS}
1	1.81e−4	1.59e−2	1.13	1.21e−4	1.64e−2	1.17	1.55e−4	8.89e−2	1.00
2	1.81e−4	1.52e−2	1.13	1.20e−4	1.58e−2	1.11	1.57e−4	8.90e−2	1.09
3	1.80e−4	1.47e−2	1.13	1.18e−4	1.52e−2	1.11	1.58e−4	8.90e−2	1.09
4	1.79e−4	1.42e−2	1.13	1.17e−4	1.47e−2	1.11	1.60e−4	8.91e−2	1.09
5	1.78e−4	1.37e−2	1.13	1.15e−4	1.42e−2	1.11	1.62e−4	8.91e−2	1.09
6	1.77e−4	1.33e−2	1.13	1.14e−4	1.39e−2	1.11	1.63e−4	8.92e−2	1.09
7	1.76e−4	1.33e−2	1.13	1.13e−4	1.40e−2	1.11	1.65e−4	8.92e−2	1.09
8	1.75e−4	1.35e−2	1.13	1.12e−4	1.41e−2	1.11	1.66e−4	8.93e−2	1.09
9	1.74e−4	1.36e−2	1.13	1.10e−4	1.43e−2	1.11	1.68e−4	8.94e−2	1.09
10	1.73e−4	1.38e−2	1.13	1.09e−4	1.44e−2	1.11	1.69e−4	8.94e−2	1.09
11	1.73e−4	1.39e−2	1.13	1.08e−4	1.45e−2	1.11	1.71e−4	8.95e−2	1.09
12	1.72e−4	1.41e−2	1.13	1.07e−4	1.47e−2	1.11	1.72e−4	8.95e−2	1.09
13	1.71e−4	1.42e−2	1.13	1.06e−4	1.48e−2	1.11	1.74e−4	8.96e−2	1.09
14	1.70e−4	1.44e−2	1.13	1.05e−4	1.49e−2	1.11	1.75e−4	8.96e−2	1.09
15	1.70e−4	1.45e−2	1.13	1.04e−4	1.51e−2	1.11	1.77e−4	8.97e−2	1.09
16	1.69e−4	1.47e−2	1.13	1.02e−4	1.52e−2	1.11	1.78e−4	8.98e−2	1.09
17	1.68e−4	1.48e−2	1.13	1.01e−4	1.54e−2	1.11	1.80e−4	8.98e−2	1.09
18	1.67e−4	1.49e−2	1.13	1.00e−4	1.55e−2	1.11	1.81e−4	8.99e−2	1.09
19	1.67e−4	1.51e−2	1.13	9.93e−5	1.56e−2	1.11	1.83e−4	8.99e−2	1.09
20	1.66e−4	1.52e−2	1.13	9.83e−5	1.57e−2	1.11	1.85e−4	9.00e−2	1.09

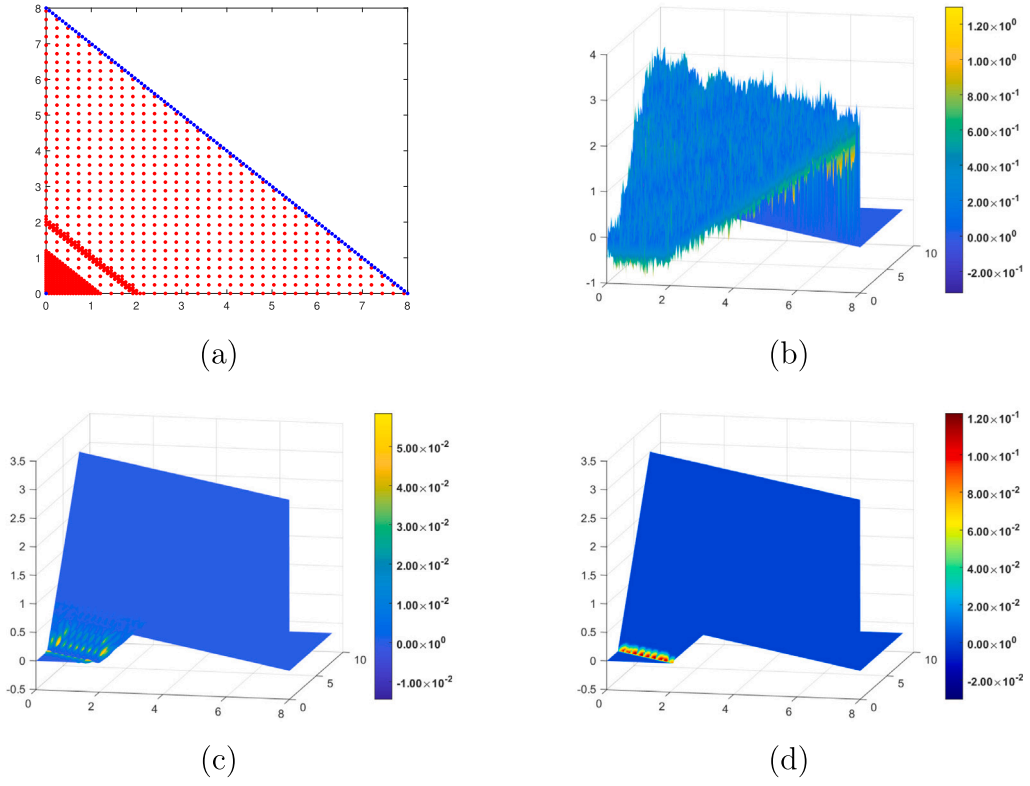

Fig. 3. (a) Locally refined node distribution near the payoff kink. Absolute error surface at the last time step for (b) the global RBF method, (c) the RBF-FD method, and (d) the MS method.

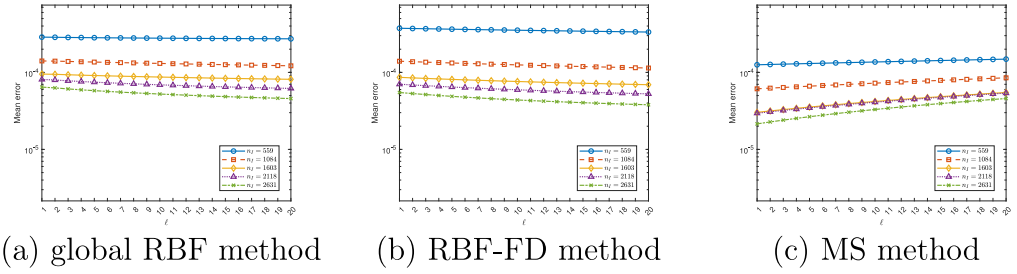

Fig. 4. Time evolution of the mean error for global RBF, RBF-FD, and MS using Halton node distributions with increasing spatial resolution.

Table 3
Mean and maximum errors computed away from the payoff kink ($\delta = 0.3$) for global RBF, RBF-FD, and MS on different node distributions at the last time step.

Node set	Method	$E_{\text{mean,away}}$	$E_{\text{max,away}}$
Halton	Global RBF	3.35e−4	2.17e−2
	RBF-FD	2.50e−4	3.36e−2
	MS	5.80e−7	2.02e−3
Uniform	Global RBF	2.18e−4	4.03e−3
	RBF-FD	6.97e−5	7.03e−3
	MS	9.57e−7	2.60e−3

Table 4
Comparison of global RBF, RBF-FD, and MS on locally refined and uniform node distributions with a similar number of collocation nodes ($n_I = 906$ and $n_I = 902$, respectively).

	E_{mean}	E_{max}	$E_{\text{mean,away}}$	$E_{\text{max,away}}$
Global RBF (Refinement)	1.41e−1	1.30e+0	2.81e−1	1.30e+0
RBF-FD (Refinement)	6.43e−4	5.83e−2	8.77e−4	5.83e−2
MS (Refinement)	5.25e−4	1.22e−1	5.78e−6	6.32e−3
Global RBF (Uniform)	9.40e−5	1.63e−2	9.49e−5	2.52e−3
RBF-FD (Uniform)	5.64e−5	1.61e−2	2.13e−5	1.01e−3
MS (Uniform)	4.96e−5	2.92e−2	5.87e−9	5.15e−6

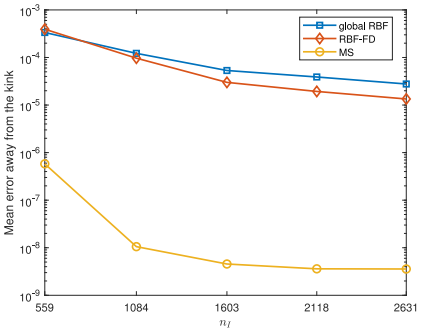

Fig. 5. Mean error away from the payoff kink as a function of the number of collocation Halton nodes for the global RBF, RBF-FD, and MS methods.

6.3.1. Temporal sensitivity

To assess the influence of the temporal discretization, we perform tests on a representative uniform node distribution with $n_I = 1224$, while keeping $T = 0.045$ fixed and varying the number of time steps $M_T = 20, 40, 80, 160$. The results in Table 5 show that the errors of global RBF, RBF-FD, and MS are essentially independent of the temporal resolution. Both global and away-from-the-kink errors remain nearly unchanged as M_T increases, indicating that the overall error is dominated by the spatial discretization rather than by the BDF2 time integration.

6.3.2. Spatial convergence

We investigate the convergence behavior of the considered methods by increasing the number of uniform nodes and evaluating the mean and maximum errors both globally and away from the payoff kink. The spatial resolution reported in Tables 6–7 is defined by $h_N = \sqrt{|\Omega|/N_I} = \sqrt{32/N_I}$, since $|\Omega| = 8^2/2 = 32$.

The global results in Table 6 show a regular decrease of the mean error for both global RBF and RBF-FD as the spatial resolution increases. RBF-FD yields slightly smaller mean errors over the tested resolutions, while the maximum errors of the two methods are very similar and decrease more slowly, approaching values of the order of 10^{-2}. The MS method exhibits a different behavior: although the global error is overall reduced on finer discretizations, both mean and maximum errors are non-monotone and show oscillations. This is consistent with the dominant influence of the low-regularity region around the payoff kink, and the global MS data should therefore not be interpreted as defining a clean asymptotic convergence rate.

Table 5
Sensitivity of the error with respect to the number of time steps ($T = 0.045$, uniform nodes with $n_I = 1224$).

Method	M_T	E_{mean}	E_{max}	$E_{\text{mean,away}}$	$E_{\text{max,away}}$
Global RBF	20	5.1130e−5	1.1862e−2	5.5714e−5	1.6165e−3
	40	5.1167e−5	1.1863e−2	5.5788e−5	1.6162e−3
	80	5.1176e−5	1.1863e−2	5.5806e−5	1.6161e−3
	160	5.1179e−5	1.1863e−2	5.5810e−5	1.6161e−3
RBF-FD	20	3.2887e−5	1.1790e−2	1.7629e−5	1.7756e−3
	40	3.2886e−5	1.1791e−2	1.7624e−5	1.7753e−3
	80	3.2885e−5	1.1791e−2	1.7623e−5	1.7752e−3
	160	3.2885e−5	1.1792e−2	1.7623e−5	1.7752e−3
MS	20	7.0689e−5	4.5166e−2	5.4700e−9	5.6675e−6
	40	7.0688e−5	4.5166e−2	3.1602e−9	5.6649e−6
	80	7.0688e−5	4.5166e−2	2.5830e−9	5.6643e−6
	160	7.0687e−5	4.5166e−2	2.4387e−9	5.6641e−6

Away from the kink, Table 7 and Fig. 6 show a clearer decay for all three methods. RBF-FD generally improves upon the global RBF approximation in this smooth region, particularly on the finer node sets. The MS error decreases much more rapidly, reaching mean errors of the order of 10^{-9} and maximum errors of the order of 10^{-7}. These very small smooth-region errors are consistent with the local polynomial reproduction properties of the MS approximation. However, they should be regarded as a diagnostic of the approximation behavior away from the low-regularity region rather than as evidence of a uniform accuracy advantage over the whole domain.

6.4. Computational cost and sparsity of the collocation matrix

To further assess the computational properties of the three methods, we report the sparsity patterns of the resulting discretization matrices together with the measured CPU times. The CPU times are reported in Fig. 7 and Table 8 as a function of the number of uniform collocation nodes. The reported values are the median over five runs. Consistently with the previous experiments, the timings include the complete computational procedure used to obtain the numerical solution at the evaluation points, including the reconstruction stage. All computations were performed in MATLAB R2024a on a machine equipped with an 11th Gen Intel Core i7-1165G7 processor at 2.80 GHz and 16 GB of RAM, running a 64-bit Windows operating system. Where explicit parallel loops are used in the implementations, they were executed with the same MATLAB thread-based parallel pool with four workers.

For the present MATLAB implementations, the global RBF method exhibits the strongest increase in computational cost as the node set is refined. The MS method is the least expensive approach over the entire range of tested node distributions. Its computational time increases with the number of nodes, but remains below that of both the global RBF and RBF-FD implementations even at the finest resolution. The RBF-FD timings show a comparatively weak dependence on the number of nodes, although the larger setup cost of the local RBF-FD discretization makes it more expensive than MS for all the node sets considered here.

The corresponding sparsity patterns are shown in Fig. 8 for $n_I = 189, 1224, 4004$. Both MS and RBF-FD lead to sparse discretization matrices, consistently with their local construction, whereas the global RBF collocation matrix is dense. Nevertheless, the two sparse methods have different local structures: the MS matrix is generated by the multinode Shepard construction, while the RBF-FD matrix is assembled from fixed local stencils. Thus, the comparison with RBF-FD separates the effect of locality and sparsity from the comparison with the global RBF benchmark.

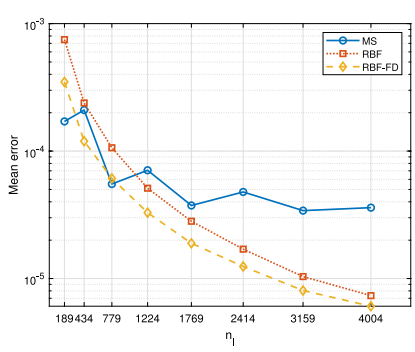

(a) global mean error

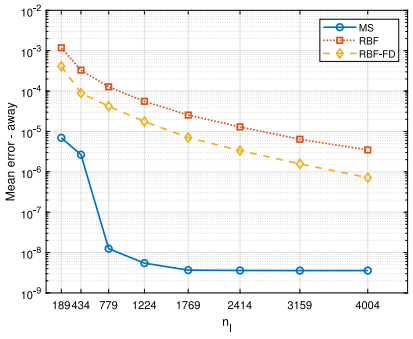

(b) mean error away from the kink

Fig. 6. Spatial convergence behavior on uniform node distributions. (a) Mean error as a function of the number of collocation nodes N_I in semilogarithmic scale. (b) Mean error computed away from the payoff kink.

Table 6
Global convergence study for global RBF, RBF-FD, and MS on increasing uniform node distributions.

N_I	h_N	E_{mean}			E_{max}		
		Global RBF	RBF-FD	MS	Global RBF	RBF-FD	MS
189	4.11e−1	7.49e−4	3.49e−4	1.71e−4	2.40e−2	2.27e−2	8.65e−2
434	2.72e−1	2.39e−4	1.20e−4	2.10e−4	1.70e−2	1.63e−2	8.57e−2
779	2.03e−1	1.06e−4	6.11e−5	5.52e−5	1.30e−2	1.29e−2	3.09e−2
1224	1.62e−1	5.11e−5	3.29e−5	7.07e−5	1.19e−2	1.18e−2	4.52e−2
1769	1.35e−1	2.82e−5	1.89e−5	3.74e−5	1.08e−2	1.07e−2	1.92e−2
2414	1.15e−1	1.70e−5	1.24e−5	4.78e−5	1.06e−2	1.06e−2	2.97e−2
3159	1.01e−1	1.04e−5	8.05e−6	3.41e−5	1.01e−2	1.02e−2	1.92e−2
4004	8.94e−2	7.34e−6	6.07e−6	3.60e−5	1.02e−2	1.02e−2	2.92e−2

Table 7
Convergence study away from the payoff kink for global RBF, RBF-FD, and MS on increasing uniform node distributions.

N_I	h_N	$E_{\text{mean,away}}$			$E_{\text{max,away}}$		
		Global RBF	RBF-FD	MS	Global RBF	RBF-FD	MS
189	4.11e−1	1.18e−3	4.10e−4	6.96e−6	1.94e−2	1.32e−2	1.01e−2
434	2.72e−1	3.30e−4	8.93e−5	2.65e−6	5.64e−3	6.54e−3	6.16e−3
779	2.03e−1	1.27e−4	4.20e−5	1.25e−8	2.98e−3	2.50e−3	1.02e−5
1224	1.62e−1	5.57e−5	1.76e−5	5.47e−9	1.62e−3	1.78e−3	5.67e−6
1769	1.35e−1	2.54e−5	7.07e−6	3.67e−9	7.91e−4	6.61e−4	2.61e−7
2414	1.15e−1	1.29e−5	3.36e−6	3.60e−9	5.15e−4	4.94e−4	2.19e−7
3159	1.01e−1	6.40e−6	1.57e−6	3.58e−9	3.32e−4	1.97e−4	1.02e−7
4004	8.94e−2	3.48e−6	7.19e−7	3.58e−9	2.12e−4	1.36e−4	1.03e−7

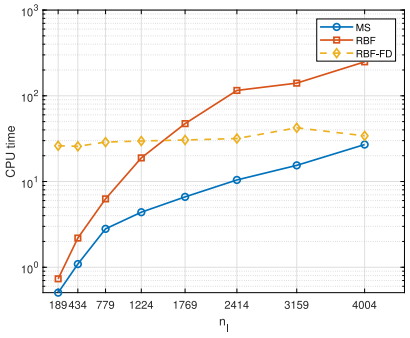

Fig. 7. CPU time as a function of the number of uniform collocation nodes n_I for the MS, global RBF and RBF-FD methods (semilog scale).

Table 8
CPU time (in seconds) for the MS, global RBF, and RBF-FD methods as a function of the number of collocation nodes. The reported values are the medians over five runs.

N_I	MS	Global RBF	RBF-FD
189	0.51	0.73	26.13
434	1.09	2.19	25.75
779	2.81	6.28	28.84
1224	4.39	18.86	29.70
1769	6.62	47.34	30.52
2414	10.43	115.46	31.72
3159	15.44	140.55	42.33
4004	27.00	248.99	34.11

7. Conclusions

This work investigates multinode Shepard collocation as a spatial discretization for a time-dependent two-dimensional Black–Scholes problem with mixed derivatives, degeneracy on the coordinate axes,

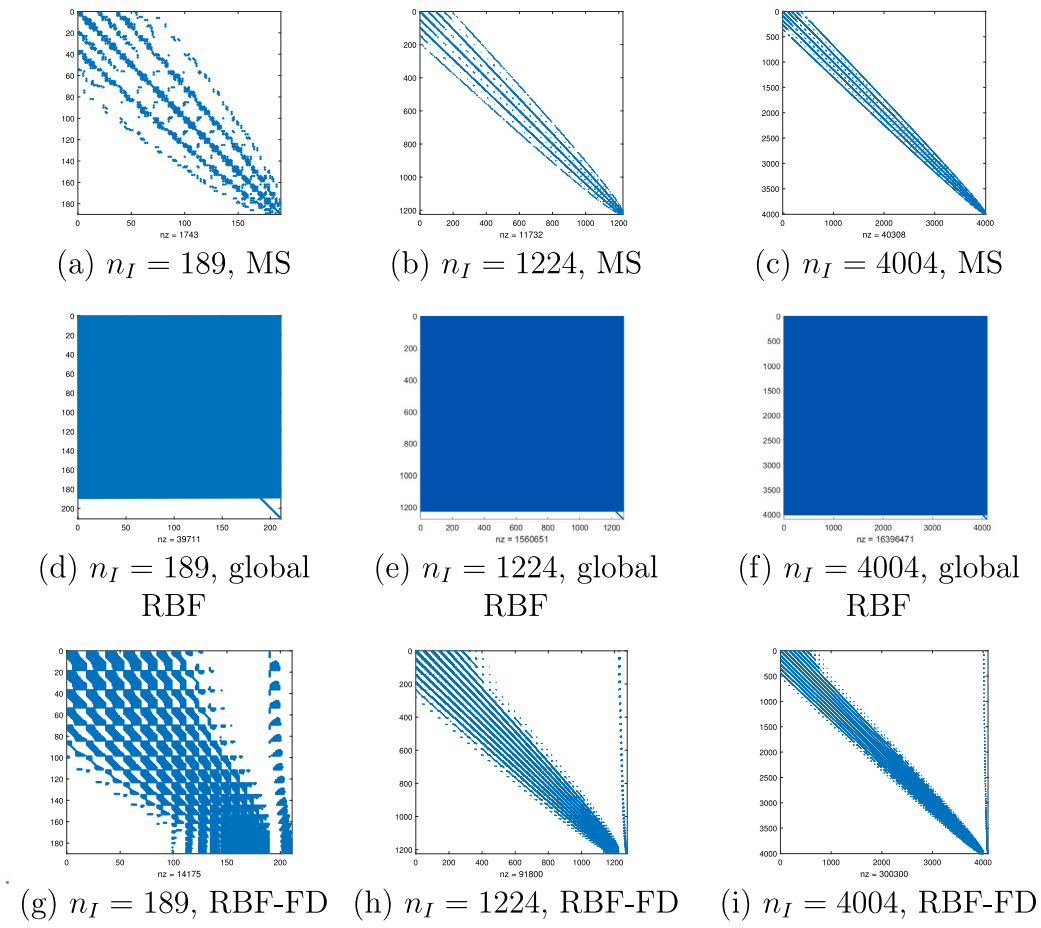

(a) $n_I = 189$, MS (b) $n_I = 1224$, MS (c) $n_I = 4004$, MS

(d) $n_I = 189$, global RBF (e) $n_I = 1224$, global RBF (f) $n_I = 4004$, global RBF

(g) $n_I = 189$, RBF-FD (h) $n_I = 1224$, RBF-FD (i) $n_I = 4004$, RBF-FD

Fig. 8. Sparsity patterns of the discretization matrices for the MS method (first row), global RBF method (second row), and RBF-FD method (third row), for increasing numbers of collocation nodes.

and an original non-smooth basket payoff. The Black–Scholes model and the BDF2 integrator are standard; the contribution of the study lies instead in assessing a spatial approximation paradigm that is structurally different from both global RBF collocation and RBF-generated finite-difference methods.

The numerical experiments identify two main features of the MS discretization. First, the global error is dominated by a narrow neighborhood of the payoff kink, so that the tested global errors do not display a clean asymptotic rate. When the same errors are evaluated away from the kink, where the solution is smooth, MS exhibits a rapid error decay and very high accuracy. Second, the MS results are comparatively insensitive to substantial changes in node geometry: similar qualitative behavior is observed on uniform layouts, scattered Halton sets, and strongly locally refined configurations.

The additional RBF-FD benchmark shows that locality and sparsity alone do not explain the numerical behavior observed for MS. On uniform node sets, RBF-FD is highly competitive in terms of global accuracy and, in the present MATLAB implementation, exhibits a favorable computational scaling as the number of nodes increases. On scattered and locally refined configurations, however, a greater sensitivity to node geometry is observed, whereas MS retains a comparatively robust behavior and a particularly high accuracy in the smooth region. The global RBF benchmark remains more sensitive to clustering and additionally requires the selection of a shape parameter.

These results do not indicate a uniform superiority of one method over the others. Rather, they show that the three spatial discretizations exhibit different numerical characteristics: global RBF provides an accurate global meshfree reference, RBF-FD combines locality and sparsity with competitive accuracy and computational cost, while MS is characterized by high smooth-region accuracy and robustness with respect to changes in node geometry. The behavior near the payoff kink remains the main limitation of the MS approximation and represents a natural direction for further investigation. Future work may therefore address problem-adapted local approximation spaces aimed at improving the accuracy in the immediate neighborhood of the kink.

CRediT authorship contribution statement

Francesco Dell'Accio: Writing – original draft, Validation, Software, Methodology, Investigation, Formal analysis, Conceptualization. **Filomena Di Tommaso:** Writing – original draft, Validation, Software, Methodology, Investigation, Formal analysis, Conceptualization. **Elisa Francomano:** Writing – original draft, Validation, Software, Methodology, Investigation, Formal analysis, Conceptualization. **Clara Lorenzi:** Writing – original draft, Validation, Software, Methodology, Investigation, Formal analysis, Conceptualization.

Declaration of competing interest

The authors declare that they have no known competing financial interests or personal relationships that could have appeared to influence the work reported in this paper.

Acknowledgments

This research has been achieved as part of RITA "Research ITalian network on Approximation", as part of the UMI group "Teoria dell'Approssimazione e Applicazioni" and was supported by INDAM-GNCS project 2025. The authors are members of the INdAM Research group GNCS.

Data availability

No data was used for the research described in the article.

References

[1] Milovanović S, von Sydow L. A high order method for pricing of financial derivatives using radial basis function generated finite differences. Math Comput Simulation 2020;174:205–17.

[2] Black F, Scholes M. The pricing of options and corporate liabilities. J Political Econ 1973;81(3):637–54.

[3] Ikamari C, Ngare P, Weke P. Multi-asset option pricing using an information-based model. Sci Afr 2020;10:e00564.

[4] Tavella D, Randall C. Pricing Financial Instruments: The Finite Difference Method. Wiley series in financial engineering, Wiley, New York; 2000.

[5] Persson J, von Persson L. Pricing European multi-asset options using a space-time adaptive FD-method. Comput Vis Sci 2007;10:173–83.

[6] Lötstedt P, Persson J, von Sydow L, Tysk J. Space–time adaptive finite difference method for European multi-asset options. Comput Math Appl 2007;53(8):1159–80.

[7] Linde G, Persson J, Von Sydow L. A highly accurate adaptive finite difference solver for the Black-Scholes equation. Int J Comput Math 2009;86(12):2104–21.

[8] Düring B, Fournié M. High-order compact finite difference scheme for option pricing in stochastic volatility models. J Comput Appl Math 2012;236(17):4462–73.

[9] Düring B, Heuer C. High-order compact schemes for parabolic problems with mixed derivatives in multiple space dimensions. SIAM J Numer Anal 2015;53(5):2113–34.

[10] In't Hout K, Foulon S. ADI finite difference schemes for option pricing in the Heston model with correlation. Int J Numer Anal Model 2010;7(2):303–20.

[11] Haentjens T, In't Hout KJ. Alternating direction implicit finite difference schemes for the Heston-Hull-White partial differential equation. J Comput Finance 2012;16(1):83.

[12] Larsson E, Åhlander K, Hall A. Multi-dimensional option pricing using radial basis functions and the generalized Fourier transform. J Comput Appl Math 2008;222(1):175–92.

[13] Pettersson U, Larsson E, Marcusson G, Persson J. Improved radial basis function methods for multi-dimensional option pricing. J Comput Appl Math 2008;222(1):82–93, Special Issue: Numerical PDE Methods in Finance.

[14] Safdari-Vaighani A, Heryudono A, Larsson E. A radial basis function partition of unity collocation method for convection–diffusion equations arising in financial applications. J Sci Comput 2015;64(2):341–67.

[15] Shcherbakov V. Radial basis function partition of unity operator splitting method for pricing multi-asset American options. BIT Numer Math 2016;56:1401–23.

[16] Shcherbakov V, Larsson E. Radial basis function partition of unity methods for pricing vanilla basket options. Comput Math Appl 2016;71(1):185–200.

[17] Milovanović S, von Sydow L. Radial basis function generated finite differences for option pricing problems. Comput Math Appl 2018;75(4):1462–81.

[18] Milovanović S. Pricing financial derivatives using radial basis function generated finite differences with polyharmonic splines on smoothly varying node layouts. arXiv preprint arXiv:1808.02365 2018.

[19] von Sydow L, Höök LJ, Larsson E, Lindström E, Milovanović S, Persson J, Shcherbakov V, Shpolyanskiy Y, Sirén S, Toivanen J, Waldén J, Wiktorsson M, Levesley J, Li J, Oosterlee C, Ruijter M, Toropov A, Zhao Y. The BENCHmarking project in option pricing. Int J Comput Math 2015;92.

[20] von Sydow L, Milovanović S, Larsson E, In't Hout K, Wiktorsson M, Oosterlee CW, Shcherbakov V, Wyns M, Leitao A, Jain S, et al. Benchop-SLV: The benchmarking project in option pricing-stochastic and local volatility problems. Int J Comput Math 2019;96(10):1910–23.

[21] Dell'Accio F, Di Tommaso F. Rate of convergence of multinode Shepard operators. Dolomites Res Notes Approx 2019;12(1):1–6.

[22] Dell'Accio F, Di Tommaso F, Nouisser O, Siar N. Solving Poisson equation with Dirichlet conditions through multinode Shepard operators. Comput Math Appl 2021;98:254–60.

[23] Dell'Accio F, Di Tommaso F, Ala G, Francomano E. Electric scalar potential estimations for non-invasive brain activity detection through multinode Shepard method. In: 2022 IEEE 21st mediterranean electrotechnical conference. MELECON, 2022, p. 1264–8.

[24] Dell'Accio F, Di Tommaso F, Francomano E. Multinode Shepard method for two-dimensional elliptic boundary problems on different shaped domains. J Comput Appl Math 2024;448:115896.

[25] Dell'Accio F, Di Tommaso F, Francomano E. The enriched multinode Shepard collocation method for solving elliptic problems with singularities. Appl Numer Math 2024;205:87–100.

[26] Li Z, Liao H-l. Stability of variable-step BDF2 and BDF3 methods. SIAM J Numer Anal 2022;60(4):2253–72.

[27] Dell'Accio F, Di Tommaso F, Hormann K. On the approximation order of triangular Shepard interpolation. IMA J Numer Anal 2015;36(1):359–79.

[28] Hull J. Options, Futures, and Other Derivatives Global Edition. Pearson Deutschland; 2021.

[29] Janson S, Tysk J. Feynman-Kac formulas for Black-Scholes-type operators. Bull Lond Math Soc 2006;38(2):269–82.

[30] Dell'Accio F, Di Tommaso F, Larosa F. The multinode Shepard method: MATLAB implementation. J Approx Softw 2024;1(2).

[31] Bos L, De Marchi S, Sommariva A, Vianello M. Computing multivariate Fekete and Leja points by numerical linear algebra. SIAM J Numer Anal 2010;48(5):1984–99.